TRUE TRIAXIAL CYCLIC LOADING TEST OF

MAHA SARAKHAM ROCK SALT

Komkrit Phatthaisong

A Thesis Submitted in Partial Fulfillment of the Requirements for the

Degree of Master of Engineering in Geotechnology

Suranaree University of Technology

Academic Year 2011

การทดสอบแรงกดแบบวัฏจักรในสามแกนจริงของเกลือหินชุดมหาสารคาม

นายคมกริช ผาดไธสง

วิทยานิพนธ์นี้เป็นส่วนหนึ่งของการศึกษาตามหลักสูตรปริญญาวิศวกรรมศาสตรมหาบัณฑิต
สาขาวิชาเทคโนโลยีธรณี
มหาวิทยาลัยเทคโนโลยีสุรนารี
ปีการศึกษา 2554

TRUE TRIAXIAL CYCLIC LOADING TEST OF

MAHA SARAKHAM ROCK SALT

Suranaree University of Technology has approved this thesis submitted in partial fulfillment of the requirements for a Master's Degree.

Thesis Examining Committee

_____

(Assoc. Prof. Kriangkrai Trisarn)

Chairperson

_____

(Assoc. Prof. Dr. Kittitep Fuenkajorn)

Member (Thesis Advisor)

_____

(Dr. Prachya Tepnarong)

Member

_____   _____

(Prof. Dr. Sukit Limpijumnong)   (Assoc. Prof. Flt. Lt. Dr. Kontorn Chamniprasart)

Vice Rector for Academic Affairs   Dean of Institute of Engineering

คมกริช ผาดไธสง : การทดสอบแรงกดแบบวัฏจักรในสามแกนจริงของเกลือหินชุด
มหาสารคาม (TRUE TRIAXIAL CYCLIC LOADING TEST OF MAHA SARAKHAM
ROCK SALT) อาจารย์ที่ปรึกษา : รองศาสตราจารย์ ดร.กิตติเทพ เฟื่องขจร, 52 หน้า.

วัตถุประสงค์ของการศึกษานี้ คือ เพื่อหาผลกระทบของแรงกดแบบวัฏจักรต่อพฤติกรรม
เชิงเวลาของเกลือหินภายใต้ความเค้นในสามแกนจริง ผลการทดสอบสามารถนำมาประยุกต์ใช้
ในการคำนวณการหดตัวของโพรงเกลือหินที่ใช้กักเก็บก๊าซธรรมชาติ ตัวอย่างที่ทดสอบถูกจัดเตรียม
มาจากเกลือหินชั้นกลางของหมวดหินมหาสารคามในภาคตะวันออกเฉียงเหนือของประเทศไทย
แท่งตัวอย่างเกลือถูกตัดและฝนให้เป็นรูปสี่เหลี่ยมลูกบาศก์ขนาด 5.4× 5.4 ×5.4 ลูกบาศก์เซนติเมตร
โครงกดในหลายแกนถูกใช้เพื่อให้ความเค้นหลักที่คงที่ต่อตัวอย่างเกลือหินสภาวะของความเค้น
ผันแปรจากความเค้นกดในสามแกน ($\sigma_1 \neq \sigma_2 = \sigma_3$) และความเค้นกดในหลายแกน ($\sigma_1 \neq \sigma_2 \neq \sigma_3$)
ความเค้นเฉือนในสามมิติถูกผันแปรจาก 2 5 8 11 ถึง 14 เมกะปาสกาล ในขณะที่ความเค้นเฉลี่ย
ถูกปรับให้คงที่เท่ากับ 15 เมกะปาสกาล การเปลี่ยนรูปร่างของตัวอย่างถูกวัดอย่างต่อเนื่อง
ในแนวแกนหลักขณะที่ทดสอบไปจนถึง 1,200 วัฏจักร รูปแบบของ Burgers ได้นำมาใช้
เพื่ออธิบายพฤติกรรมเชิงยืดหยุ่น พฤติกรรมยืดหยุ่นเชิงเวลา และพฤติกรรมพลาสติกเชิงเวลา
ผลที่ได้ระบุว่าสัมประสิทธิ์ความยืดหยุ่นของเกลือหินจะไม่ขึ้นกับวัฏจักรของการกด แต่คุณสมบัติ
แบบพลาสติกเชิงเวลาจะขึ้นกับวัฏจักรของการกด โดยมีค่าต่ำกว่าผลที่ได้จากการทดสอบแบบ
สถิตประมาณ 10 เท่า ส่งผลให้การคำนวณการยุบตัวของโพรงกักเก็บภายใต้แรงกดแบบวัฏจักรจะมี
ค่าสูงกว่าผลที่ได้จากการคำนวณ โดยใช้ผลการทดสอบภายใต้แรงดันสถิต ซึ่งผลการศึกษานี้ระบุว่า
การทดสอบแบบใช้แรงดันสถิตที่ใช้กันอยู่ในปัจจุบันจะให้ผลการประเมินเสถียรภาพในเชิง
ไม่อนุรักษ์

KOMKRIT PHATTHAISONG : TRUE TRIAXIAL CYCLIC LOADING

TEST OF MAHA SARAKHAM ROCK SALT. THESIS ADVISOR :

ASSOC. PROF. KITTITEP FUENKAJORN, Ph.D., P.E., 52 PP.

ROCK SALT/CREEP/CYCLIC LOADING/POLYAXIAL LOADING

The objective of this study is to determine the effects of cyclic loading on the time-dependent behavior of rock salt under true triaxial stresses. The results are applied to determine the creep closure of natural gas storage caverns in rock salt formation. The salt specimens are obtained from the Middle member of the Maha Sarakham formation in the northeast of Thailand. The salt cores are cut and ground to obtain cubical shaped specimens with nominal dimensions of $5.4 \times 5.4 \times 5.4$ cm^3. A polyaxial load frame is used to apply constant principal stresses to the salt specimens. The applied stresses are varied from the triaxial ($\sigma_1 \neq \sigma_2 = \sigma_3$) condition to the polyaxial ($\sigma_1 \neq \sigma_2 \neq \sigma_3$) conditions. The applied octahedral shear stresses vary from 2, 5, 8, 11 to 14 MPa while the mean stress is maintained constant at 15 MPa for all specimens. The specimen deformations are monitored along the three principal axes for up to 1200 cycles. The Burgers model is used to describe the elastic, visco-elastic (transient) and visco-plastic (steady-state) behavior of the salt. Regression analyses on the octahedral shear strain-time curves suggest that the salt elastic modulus tends to be independent of the cyclic loads. In the steady-state creep phase, the visco-plastic parameter calibrated from the true triaxial cyclic loading test is about an order of magnitude lower than those under true triaxial static loading. Cavern closure simulated using parameters calibrated from the cyclic loading test results are greater

than those from the static loading results. This suggests that application of the property parameters obtained from the conventional static loading creep test to assess the stability of the storage caverns with internal pressure fluctuation may not be conservative.

School of Geotechnology   Student's Signature_____

Academic Year 2011   Advisor's Signature_____

ACKNOWLEDGMENTS

Komkrit Phatthaisong

TABLE OF CONTENTS

TABLE OF CONTENTS (Continued)

TABLE OF CONTENTS (Continued)

LIST OF TABLES

SYMBOLS AND ABBREVIATIONS

E	=	Young's modulus
E_1	=	Elastic modulus
E_2	=	Visco-elastic parameter
F	=	Load on rock sample
L	=	Specimen length
t	=	Time
W	=	Weight on bars
ε_1	=	Strain in maximum principal stress direction
ε_2	=	Strain in intermediate principal stress direction
ε_3	=	Strain in minimum principal stress direction
ε_V	=	Volumetric strain
γ_{oct}	=	Octahedral shear strain
η_1	=	Visco-plastic Parameter
η_2	=	Visco-elastic Parameter
ρ	=	Rock Density
σ_1	=	Maximum Principal Stress
σ_2	=	Intermediate principal Stress
σ_3	=	Minimum Principal Stress
σ_m	=	Mean stress
τ_{oct}	=	Octahedral Shear Stress

CHAPTER I

INTRODUCTION

1.1 Background and rationale

Rock salt around storage caverns will subject to cycles of loading due to the fluctuation of cavern pressures during product injection and retrieval periods. The internal pressures depend on the types of the stored products (e.g. petroleum, liquefied gas or compressed-air). A difficulty arise in determining the representative properties of the salt under such cyclic loading states. Since the salt properties are loading path dependent (non-linear), the laboratory determined properties under static loads (as commonly practiced) may not truly represent the actual in-situ salt behavior under cyclic loading. The effects of confining pressures at great depths on the creep properties of rocks are commonly simulated in a laboratory by performing triaxial creep testing of cylindrical rock core specimens. A significant limitation of these conventional methods is that the intermediate and minimum principal stresses are equal during the test while the actual in-situ rock is normally subjected to an anisotropic stress state where the maximum, intermediate and minimum principal stresses are different ($\sigma_1 \neq \sigma_2 \neq \sigma_3$). It has been commonly found that compressive strengths obtained from conventional triaxial testing can not represent the actual in-situ strength where the rock is subjected to an anisotropic stress state. In particular, the study of the salt creep behavior under true triaxial cyclic loading has never been attempted.

1.2   Research objectives

The objective of this research is to determine the effect of cyclic loading on the time-dependent behavior of rock salt under true triaxial stresses. A polyaxial load frame is used to apply cycles of principal stresses to the cubical salt speciems. The applied stresses are varied from the triaxial ($\sigma_1 \neq \sigma_2 = \sigma_3$) condition to the polyaxial ($\sigma_1 \neq \sigma_2 \neq \sigma_3$) conditions. The applied octahedral shear stresses (τ_{oct}) vary from 2, 5, 8, 11 to 14 MPa while the mean stress (σ_m) is maintained constant at 10,15 and 20 MPa. The results will be used to calibrate the elastic, visco-elastic and visco-plastic parameters of the rock and compared with those determined from the conventional static loading creep tests.

1.3   Research methodology

The research methodology shown in Figure 1.1 comprises 7 steps; including literature review, sample preparation, polyaxial cyclic loading testing, calibration of Burgers Parameters, computer simulation, discussions and conclusions and thesis writing.

1.3.1   Literature review

Literature review is carried out to study the previous researches on time-dependent behavior of rock salt in true-triaxial state and the effect of intermediate principal stress. The sources of information are from text books, journals, technical reports and conference papers. A summary of the literature review is given in the thesis.

1.3.2 Sample preparation

Rock samples used here have been obtained from the Middle members of the Maha Sarakham formation in the northeastern Thailand. The rock salt is relatively pure halite. Sample preparation is carried out in the laboratory at Suranaree University of Technology. Samples prepared for the polyaxial cyclic loading test are $5.4 \times 5.4 \times 5.4 \text{ cm}^3$.

1.3.3 Polyaxial cyclic loading test

The laboratory testing involves true triaxial cyclic loading tests in polyaxial load frame. A polyaxial load frame is shown in Figure 1.2. A polyaxial load frame equipped with two pairs of cantilever beams and install hydraulic load cell will be used to apply axial stress (σ_1) and lateral stresses (σ_3) to the salt specimen while lateral stresses (σ_2) will be applied by a hydraulic load cell. The specimen was first confined under hydrostatic stress equivalent to the pre-defined mean stress (σ_m). One of the lateral stresses was then decreased to the pre-defined minimum principal stress while the axial stress was increased pre-defined maximum principal stress under 30 second later axial stress (σ_1) was decreased to the mean stress (σ_m) and lateral stresses (σ_3) was increased to the mean stress (σ_m) under 30 second Called 1 cycle.

1.3.4 Calibration of Burgers parameters

The test results are used to calibrate the elastic, visco-elastic and visco-plastic parameters of the rock. It is assumed here that the salt behavior can be described by the Burgers model. The regression analysis on the linear visco-elastic equation will be made on the test data.

1.3.5 Computer simulations

A finite element analysis with the creep model above is performed to demonstrate the impact of cyclic loading on the salt behavior around a compressed-air storage cavern subject to cycles of pressure injection and retrieval.
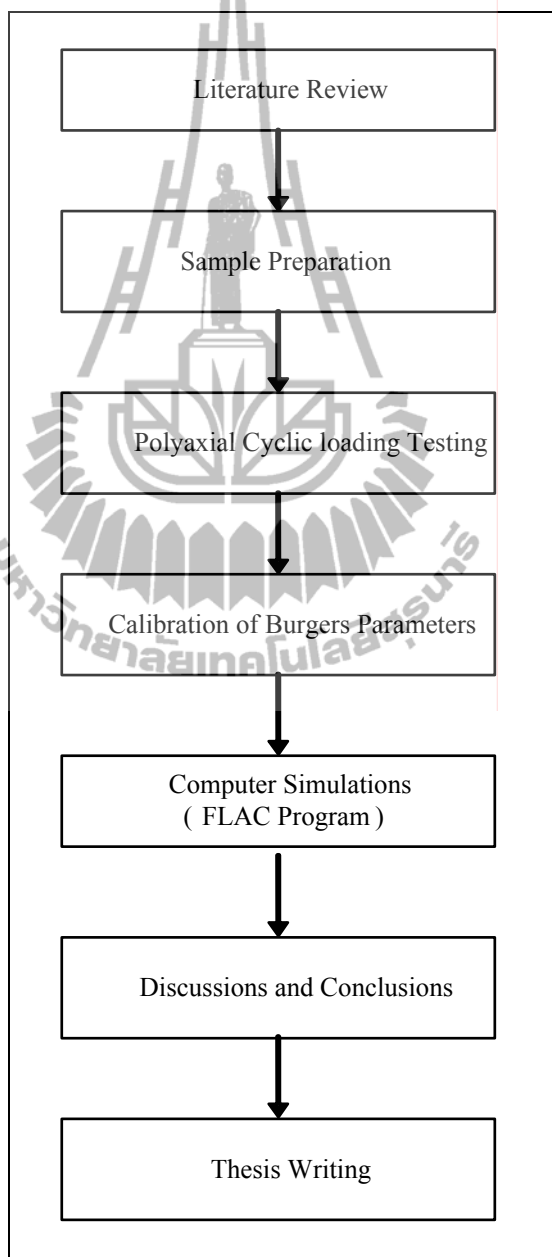
Figure 1.1 Research methodology
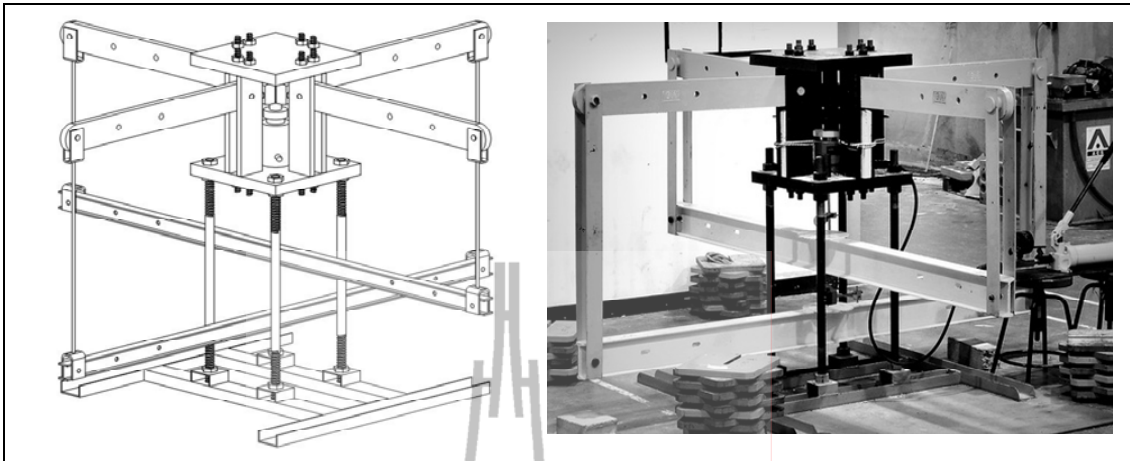
Figure 1.2 Polyaxial load frame

1.3.6 Conclusion and thesis writing

All research activities, methods, and results are documented and complied in the thesis.

1.4 Scope and limitations

The scope and limitations of the research include as follows.

1. Laboratory experiments are conducted on rock salt specimens from the Maha Sarakham formation.

2. The applied mean stresses (σ_m) vary from 10, 15 to 20 MPa.

3. The applied octahedral shear stresses (τ_{oct}) vary from 5, 8, 11 to 14 MPa.

4. All tests are performed using loading frequencies is 0.016 Hz.

5. All tests are performed for 1200 cycles.

6. Up to 20 samples are tested, with the nominal sample sizes of 5.4×5.4× 5.4 cm^3.

7. All tests are conducted under ambient temperature.

8. Testing is made under dry condition.

9. No field testing is performed.

10. The research findings are published in conference paper or journal.

1.5   Thesis contents

This research thesis is divided into seven chapters. The first chapter includes background and rationale, research objectives, research methodology, and scope and limitations. **Chapter II** presents results of the literature review to improve an understanding of rock salt on time-dependent behavior.   **Chapter III** describes the sample preparation. **Chapter IV** describes the Polyaxial Cyclic loading Test. **Chapter V** presents Burgers parameters results from calibration. **Chapter VI** presents results computer simulations. **Chapter VII** is the discussions, conclusions and recommendations for future studies.

CHAPTER II

LITERATURE REVIEW

2.1 Introduction

This chapter summarizes the results of literature review carried out to improve an understanding of rock salt behaviour. The topics reviewed here include mechanical constitutive laws of rock salt, effects of grain size and inclusions and effect of polyaxial loading on salt behavior.

2.2 Salt behavior

Researchers from the field of material sciences believe that rock salt behaviour shows many similarities with that of various metals and ceramics (Chokski and Langdon, 1991; Munson and Wawersik, 1993). However, because alkali halides are ionic materials, there are some important differences in their behavior. Aubertin et al. (1992, 1993, 1998, 1999) conclude that the rock salt behavior should be brittle-to ductile materials or elastic-plastic behavior. This also agrees with the finding by Fuenkajorn and Daemen (1988); Fokker and Kenter (1994) and Fokker (1995, 1998). Jeremic (1994) discusses the mechanical characteristics of the salt. They are divided into three characteristics: the elastic, the elastic-plastic, and the plastic behavior. The elastic behavior of rock salt is assumed to be linearly elastic with brittle failure. The rock salt is observed as linear elastic only for a low magnitude of loading. The range of linear elastic mainly depends on the content of elastic strain and can be used to formulate the modulus of elasticity. Normally, the modulus of elasticity of rock salt is

relatively low. The elastic and plastic behavior of rock salt can be investigated from the rock salt specimen. The confined rock salt specimen at the beginning of incremental loading shows linear elastic deformation but with further load increases the plastic behavior is induced, which continues until yield failure. Elastic deformation and plastic deformation are considered as separated modes of deformability in the great majority of cases. The salt material simultaneously exhibits both elastic strain and plastic strain. The difference between elastic behavior and plastic behavior is that elastic deformation is temporary (recoverable) and plastic deformation is permanent (irrecoverable). The degree of permanent deformation depends on the ratio of plastic strain to total strain. The elastic and plastic deformation can also be observed by short-term loading, but at higher load magnitude. The plastic behavior of rock salt does not occur if the applied stress is less than the yield stress. The rock salt is deformed continually if the high stress rate is still applied and is more than the yield stress. Increasing the load to exceed the strain limit of the rock salt beyond its strength causes it to fail. The deformation of 16 rocks salt by the increase of temperature can also result in the transition of brittle-to-ductile behavior.

The time-dependent deformation (or creep) is the process at which the rock can continue deformation without changing stress. The creep strain seldom can be recovery fully when loads are removed, thus it is largely plastic deformation. Creep deformation occurs in three different phases, as shown in Figure 2.1, which relatively represents a model of salt properties undergoing creep deformation due to the sustained constant load. Upon application of a constant force on the rock salt, an instantaneous elastic strain (ε_e) is induced. The elastic strain is followed by a primary or transient strain, shown as Region I. Region II, characterized by an almost constant

slope in the diagram, corresponds to secondary or steady state creep. Tertiary or accelerating creep leading to rather sudden failure is shown in Region III. Laboratory investigations show that removal of applied load in Region I at point L will cause the strain to fall rapidly to the M level and then asymptotically back to zero at N. The distance LM is equal to the instantaneous strain ε_e. No permanent strain is induced here. If the removal of stress takes place in the steady-state phase the permanent strain (ε_p) will occur. From the stability point of view, salt structure deformations after constant load removal have only academic significance, since the stresses imposed underground due to mining operations are irreversible. The behavior of the salts with time-dependent deformation under constant load is characterized as a visco-elastic and visco-plastic phenomenon. Under these conditions the strain criteria are superior to the strength criteria for design purposes, because failure of most salt pillars occurs during accelerated or tertiary phase of creep, due to the almost constant applied load. The dimensions of a pillar in visco-elastic and visco-plastic rock should be established on the basis of a prediction of its long-term strain, to guard against adequate safety factor accelerating creep (Fuenkajorn and Daemen, 1988; Dusseault and Fordham, 1993; Jeremic, 1994; Knowles et al., 1998).
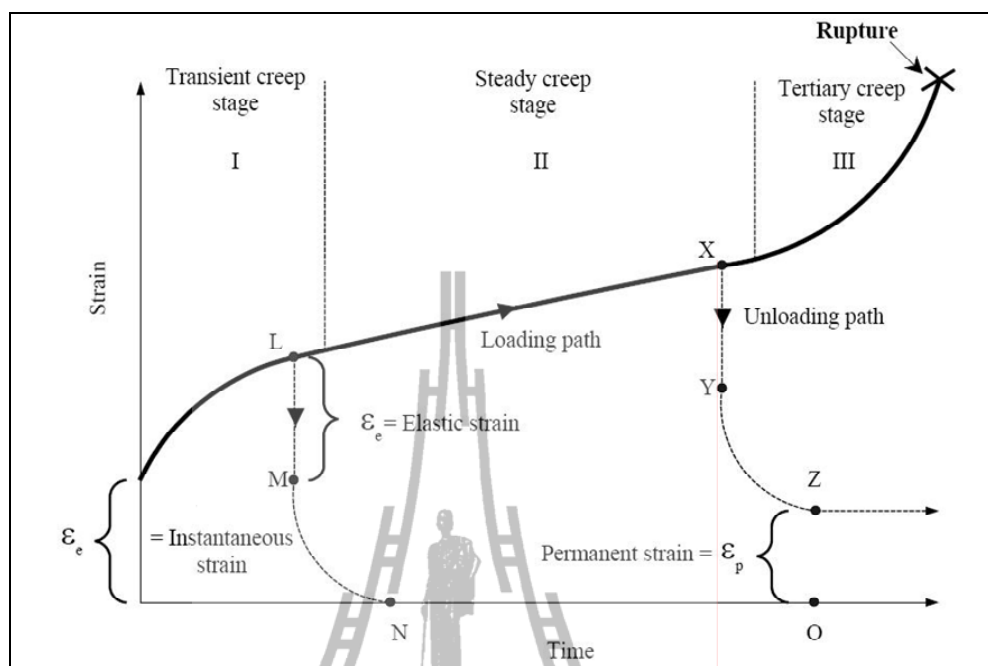
Figure 2.1 The typical deformation as a function of time of creep materials

(modified from Jeremic, 1994).

Samsri et al. (2010) determine the effect of the intermediate principal stress on the time-dependent behavior of rock salt obtained from the Maha Sarakham formation. A polyaxial creep frame applies constant principal stresses to cubical shaped specimens with a nominal dimension of $5.4 \times 5.4 \times 5.4$ cm^3. The applied octahedral shear stresses (τ_{oct}) vary from 5, 8, 11 to 14 MPa while the mean stress (σ_m) is maintained constant at 15 MPa for all specimens. The loading conditions range from the triaxial ($\sigma_1 \neq \sigma_2 = \sigma_3$) to the polyaxial ($\sigma_1 \neq \sigma_2 \neq \sigma_3$ and $\sigma_1 = \sigma_2 \neq \sigma_3$) stress states. The Burgers model is used to describe the elastic, visco-elastic (transient) and visco-plastic (steady-state) behavior of the salt. The specimen deformations are monitored along the three principal axes for up to 21 days. Regression analyses on the octahedral shear strain - time curves suggest that the salt elastic modulus tends to

be independent of the intermediate principal stress (σ_2). It however tends to increase as the applied τ_{oct} increases. Under the same magnitude of τ_{oct} the visco-elastic and visco-plastic parameters increases when σ_2 increases from the triaxial condition, $\sigma_2=\sigma_3$, to the condition where $\sigma_2=\sigma_1$.

Fuenkajorn and Phueakphum (2010) perform cyclic loading tests on the Maha Sarakham salt. Their results indicate that the salt compressive strength decreases with increasing number of loading cycles, which can be best represented by a power equation. The salt elastic modulus decreases slightly during the first few cycles, and tends to remain constant until failure. It seems to be independent of the maximum loads. Axial strain–time curves compiled from loci of the maximum load of each cycle apparently show a time-dependent behavior similar to that of creep tests under static loading. In the steady-state creep phase, the visco-plastic coefficients calculated from the cyclic loading test are about an order of magnitude lower than those under static loading. The salt visco-plasticity also decreases with increasing loading frequency. Surface subsidence and cavern closure simulated using parameters calibrated from cyclic loading test results are about 40% greater than those from the static loading results. This suggests that application of the property parameters obtained from the conventional static loading creep test to assess the long-term stability of storage caverns in salt with internal pressure fluctuation may not be conservative.

2.3 Mechanical Constitutive Laws of Rock Salt

Several mechanical constitutive laws of rock salt have been developed, which vary from simple visco-elastic models to complex dislocation theory models. Most of the laws emphasize long-term mechanical behavior under a variety of pressures and

temperatures. The constitutive models for salt can be divided into three groups: (1) rheological model, (2) empirical model, and 3) physical model.

The rheological models describe the mechanical behavior of salt, but ignore the actual mechanisms of deformation. The deformational characteristics are assumed to be governed by two basic physical elements: spring elasticity and dashpot viscosity. The mechanical behavior of salt is modeled by a combination of these elements. Since the structure of the rheological models is not related to any particular test, the model can be applied to general problems of time-dependent behavior without requiring additional assumptions. The theories of rheological models have been studied by Jin and Cristescu (1998), Cristescu (1993a, 1993b, 1994a, 1994b, 1996), Serata and Fuenkajorn (1992a), Fuenkajorn and Serata (1992, 1994), Stormont and Fuenkajorn (1994), and Massier (1996).

The empirical models are generally arbitrary functions formulated to fit a set of experimental results. Similar to the rheological approach, the development of the empirical laws ignores the actual mechanism of deformation of salt. By fitting curves to a set of data, certain relationships among the data can be established. The empirical laws can be presented in several forms (power, exponential, polynomial, etc.), depending upon the characteristics of the data. Several forms of empirical model can be studied from Fokker and Kenter (1994), Pudewills and Hornberger (1996).

The physical models start from the analysis of the microscopic structural variation of the material observed under loading, and incorporate a theoretical explanation of the basis of time-dependent behavior. The method originated in metallurgy is later introduced into rock mechanics. Rocks, however, are more complex materials than metals. The atomic bonds in natural rocks are always a

chemical bond rather than a metallic bond. Furthermore, most rocks are multigranular-structured in contrast to the relatively single phase structure of metals. The physical models are therefore considered inappropriate for describing the time-dependent behavior of rock salt (Aubertin, 1996; Aubertin et al., 1998, 1999; Korthaus, 1996, 1998).

2.4   Effect of grain size and inclusions

The effects of grain size on the creep behavior and strength of rock salt in laboratory and field conditions are described by Fokker (1998). The average grain size of salt visually observed from the core and post-failure specimens is 5 mm × 10 mm × 10 mm. It is concluded that the large size of the salt crystals increases the effect of the crystallographic features (i.e. cleavage planes) on the mechanics of deformation and failure of the samples. This also agrees with the finding by Aubertin (1996). The dislocations and plastic flows in single crystals of halite are studied by several researchers (Franssen and Spiers, 1990; Raj and Pharr, 1992; Senseny et al., 1992; Wanten et al., 1996). They conclude that the shear strength and deformation of halite crystals are orientation-dependent. The small size of the sample may not provide good representative test results. This also reflects on the specifications by ASTM (ASTM D2664, D2938 and D3967). The ASTM standard methods specify that to minimize the effect of grain size the sample diameter should be at least ten times the average grain size.

Inclusions and impurities in salt have an effect on to the creep deformation and strength of salt. The degree of impurity is varying for different scales of the rock salt. On a small scale, such as for laboratory specimens, the impurities of salt involve ferruginous inclusions and thin clay seams along grain boundaries or bedding planes.

The impurities distribute uniformly in the salt may affect the strength of rock salt. This can decrease the creep deformation and strength of rock salt. These phenomena have been reported by Franssen and Spiers (1990), Raj and Pharr (1992) and Senseny et al. (1992), as well.
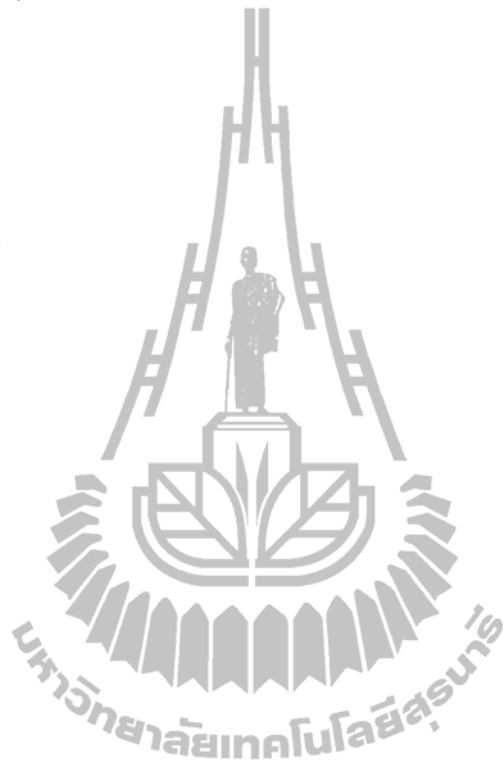
CHAPTER III

SAMPLE PREPARATION

This chapter describes sample preparation and specifications of the tested rock salt specimens. The method follows as much as practical the standard practices. The salt specimens tested here are obtained from a borehole of Pimai salt Co., Ltd., Nakhon Ratchasima province. They are from the Middle members of the Maha Sarakham (MS) formation in the northeastern Thailand. This salt member has long been considered as a host rock for compressed-air energy storage by the Thai Department of Energy. The core specimens are dry cut and ground, as shown in Figure 3.1. The core specimens with a nominal diameter of 100 mm were drilled from depths ranging between 170 and 270 m. The salt specimens have nominal dimensions of $5.4 \times 5.4 \times 5.4$ cm^3, as shown in Figure 3.2. The rock salt is relatively pure halite with slight amount (less than 1-2%) of anhydrite, clay minerals and ferrous oxide. The average crystal (grain) size is about $5 \times 5 \times 10$ mm^3. Warren (1999) gives detailed descriptions of the salt and geology of the basin. Sample preparation is conducted in the laboratory facility at the Suranaree University of Technology. A total of 30 specimens were prepared for testing. Table 3.1 summarizes the specimen depth, dimensions and density.

Figure 3.1 A salt specimen is dry cut by a cutting machine

Figure 3.2 Some salt specimens prepared for true triaxial cyclic loading test.

The nominal dimensions are $5.4 \times 5.4 \times 5.4$ cm^3.

Table 3.1 Specimen dimensions prepared for true triaxial cyclic loading test.

Specimen (mm)	Depth (m)	Width (mm)	Length (mm)	Height (mm)	weight (g)	Density (g/cc)
MS-PCL-05	161.16-160.22	57.2	56.7	57.0	408.5	2.21
MS-PCL-08	234.51-234.57	57.9	58.8	58.0	433.3	2.20
MS-PCL-16	140.13-140.19	54.6	54.8	55.8	391.5	2.34
MS-PCL-19	207.45-207.51	56.6	55.0	55.5	396.2	2.29
MS-PCL-27	234.39-234.45	55.0	54.6	55.8	376.8	2.24
MS-PCL-30	160.10-160.16	55.7	56.3	58.0	402.2	2.21
MS-PCL-11	103.89-103.95	56.9	55.2	57.4	382.4	2.12
MS-PCL-22	227.26-207.33	55.3	55.0	55.5	385.8	2.29
MS-PCL-04	204.40-204.46	56.8	57.8	57.0	406.6	2.17
MS-PCL-10	274.35-274.41	57.0	56.9	57.5	408.3	2.19
MS-PCL-15	104.07-104.13	55.0	56.8	56.8	372.8	2.10
MS-PCL-21	103.18-103.24	55.4	54.3	55.0	377.8	2.28
MS-PCL-26	144.32-144.38	55.3	56.6	55.5	378.7	2.18
MS-PCL-02	159.98-160.04	56.3	57.8	55.0	387.6	2.18
MS-PCL-13	234.57-234.63	55.8	55.0	55.2	395.0	2.33
MS-PCL-24	204.59-204.65	54.3	55.1	55.3	380.2	2.30
MS-PCL-06	274.53-274.59	55.9	56.7	57.9	392.4	2.14
MS-PCL-07	159.92-159.98	57.2	57.2	57.5	416.0	2.21
MS-PCL-17	159.86-159.92	56.3	54.0	55.2	394.2	2.35
MS-PCL-18	274.29-274.35	56.2	56.8	54.9	394.2	2.25
MS-PCL-28	234.27-234.33	55.1	56.0	55.5	381.4	2.23
MS-PCL-29	159.8-159.74	55.8	57.2	57.9	395.9	2.14
MS-PCL-03	160.22-160.28	56.9	57.3	56.7	402.1	2.18
MS-PCL-14	202.87-202.93	55.3	56.0	55.2	394.6	2.31
MS-PCL-25	160.10-160.16	55.7	56.9	58.0	402.2	2.19
MS-PCL-09	234.69-234.75	56.9	58.0	57.2	406.3	2.16
MS-PCL-20	234.94-235.0	55.8	56.4	54.2	397.3	2.33
MS-PCL-01	160.04-160.10	55.3	57.9	57.3	410.1	2.24
MS-PCL-12	144.20-144.26	56.1	55.3	55.0	397.7	2.33
MS-PCL-23	234.45-234.51	57.2	55.9	55.4	402.7	2.27

CHAPTER IV

LABORATORY TESTING

4.1 Introduction

The objective of this chapter is to experimentally determine the time-dependent properties of the Maha Sarakham salt under true triaxail cyclic loads. This chapter describes the equipment, the method and results of the tests.

4.2 Test equipment

Figure 4.1 shows the polyaxial load frame developed to apply cycles of lateral and axial stresses to the cubical salt specimen. Neoprene sheets are used to minimize the friction at all interfaces between the loading platen and the rock surface. Figure 4.2 shows the applied principal stress directions on the specimen. Two pairs of cantilever beams are used to apply the loads in mutually perpendicular directions (Figure 4.3.) The outer end of each opposite beam is pulled down by dead weight placed and load cell on a lower steel bar linking the two opposite beams underneath. The inner end is hinged by a pin mounted on vertical bars on each side of the frame. During testing all beams are arranged in nearly horizontal, and hence a compressive load results on the specimen placed at the center of the frame. Due to the different distances from the pin to the outer weighting point and to the inner loading point, a load magnification of 11 to 1 is obtained. This loading ratio is also used to determine the lateral deformation of the specimen by monitoring the vertical movement of the two steel bars below. The maximum lateral load is designed for 100 kN. The axial

load is applied by a 1000-kN hydraulic load cell. The load frame can accommodate specimen sizes from 2.5×2.5×2.5 cm to 10×10×20 cm. By adjusting the distances between the opposite loading platens different specimen sizes and shapes can be tested. Figure 4.4 plots the calibrated curves for use in polyaxial compression test. The parameter F is the load on the rock sample (kN), and W is the weight on the lower bars (kN).
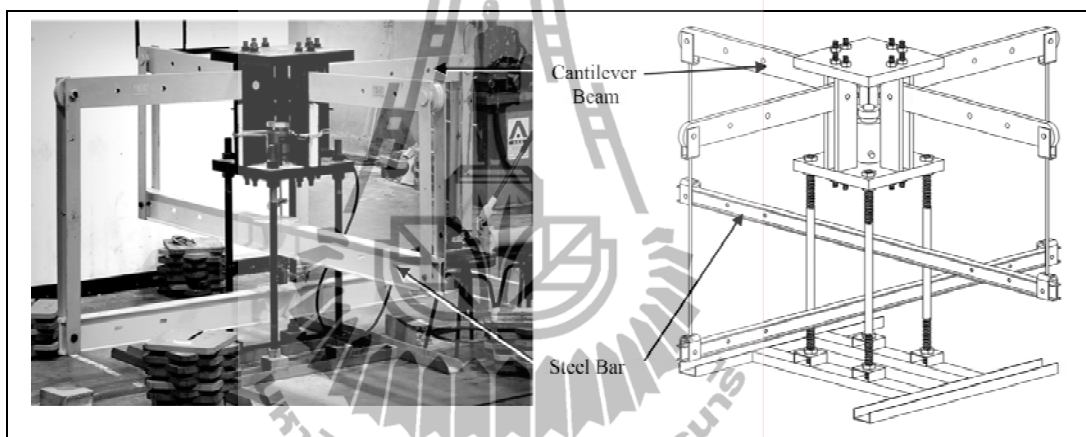

Figure 4.1 Polyaxial load frame developed for compressive strength testing

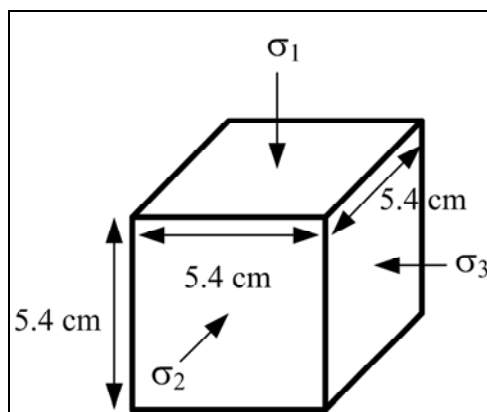under true triaxial stresses (from Walsri et al., 2009).

Figure 4.2 Directions of loading with respect to specimen shape.

4.3   Triaxial Cyclic loading tests

4.3.1   Test Procedure

The prepared rock specimen has a nominal dimension of 5.4×5.4×5.4 cm^3. The test produce can be described as follows:

1.   Place neoprene sheet on six sides of rock specimen.

2.   Connect hydraulic pump with hydraulic cylinder and check level of oil in the pump.

3.   The rock specimen with neoprene is placed on the loading platen.

4.   The lateral loading platens contacts are adjusted to the sides of specimen.

5.   Raise the cantilever beam in N–S direction.

6.   Place the rock specimen with neoprene and lateral loading platen into the polyaxial load frame.

7.   Ensure that the lateral loading platens be straight with half spherical bolt.

8.   Slowly lowering the level of the cantilever beams until half spherical bolts and lateral loading platen are in contact.

9.   Raise the cantilever beam in W–E direction.

10.   Place the lateral loading platens on the sides of specimen.

11.   Slowly lowering level of the cantilever beams.

12.   Place the loading platens on top and bottom of the specimen.

13.   Increase oil pressure using hydraulic pump until specimen, loading platens and upper steel plates are in contact.
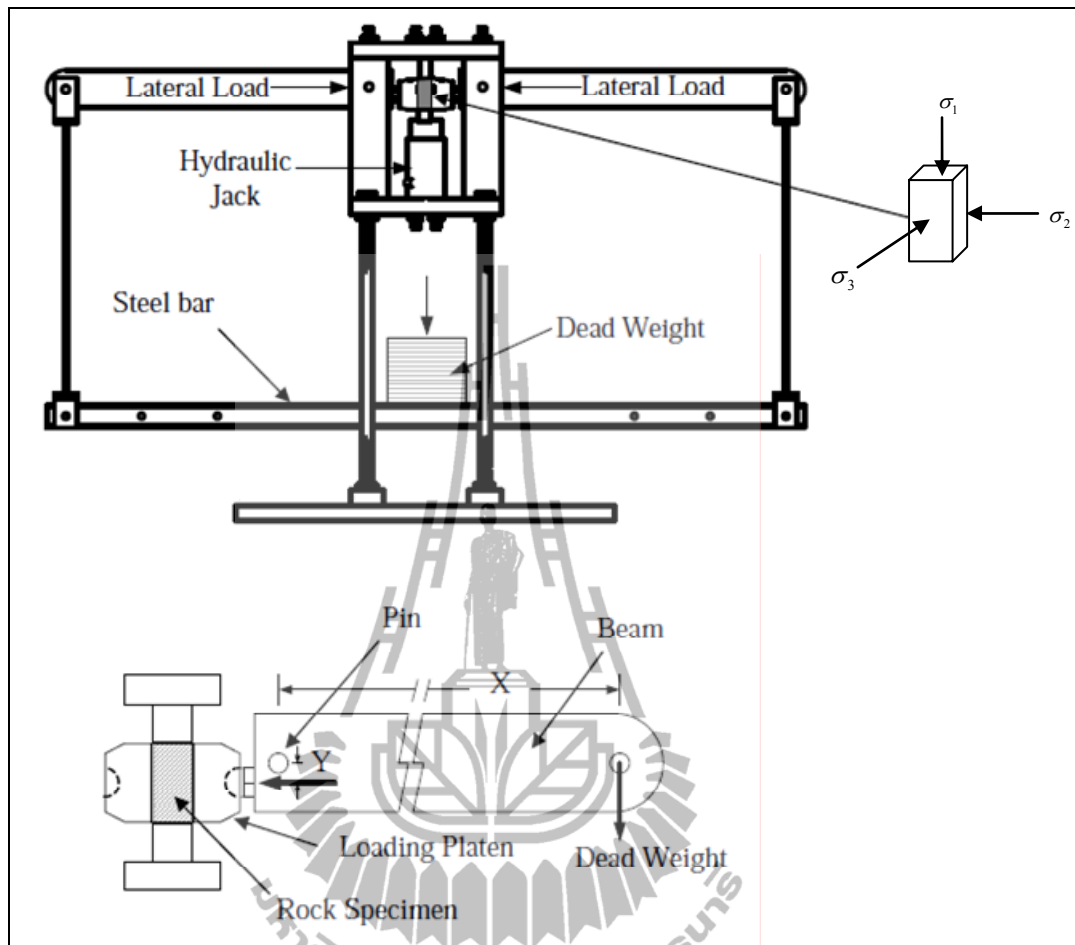
Figure 4.3 Cantilever beams weighed at outer end applies lateral stress to the rock
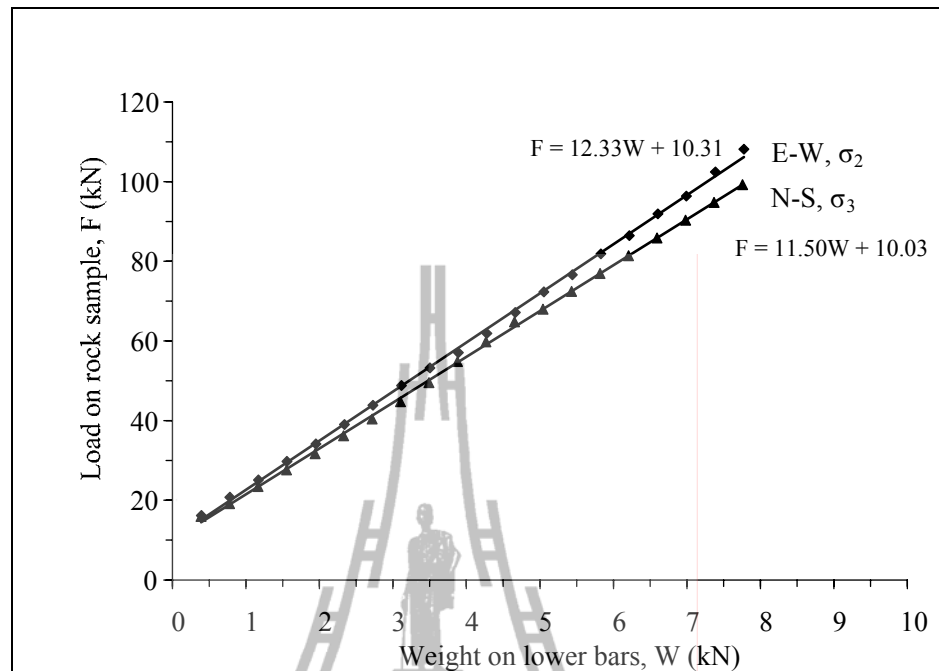
specimen (from Walsri et al., 2009).

Figure 4.4 Calibrated curves for use in polyaxial compression testing.

14. Put a steel plate (dead weight) on the middle of each beam to increase load and fix beam together.

15. Install hydraulic load cell under the middle of lower beam to apply cycles of load to cubical salt specimens.

16. The specimen was first confined under hydrostatic stress equivalent to the pre-defined mean stress (σ_m).

17. The lateral stresses were then decreased to the pre-defined minimum principal stress (by hydraulic load cell under the middle of lower beam) while the axial stress was increased pre-defined maximum principal stress (by axial hydraulic load cell) with in 30 seconds, then axial stress (σ_1) were decreased to the mean stress (σ_m) and lateral stresses (σ_3) was increased to the mean stress (σ_m) with in 30 seconds to complete one cycle.

18. The displacement digital gages are read every 30 seconds

4.3.2 Calculation

The applied stresses are then changed to obtain the pre-defined octahedral shear stresses (τ_{oct}) while maintaining the mean normal stress (σ_m) of 15 MPa (Table4.1), where τ_{oct} and σ_m are defined as:

$$\tau_{oct} = [1/3][((\sigma_1 - \sigma_2)^2 + (\sigma_1 - \sigma_3)^2 + (\sigma_2 - \sigma_3)^2)^{1/2}] \qquad (4.1)$$

$$\sigma_m = (\sigma_1 + \sigma_2 + \sigma_3) / 3 \qquad (4.2)$$

where σ_1 is maximum principal stress, σ_2 is intermediate principal stress, σ_3 is minimum principal stress.

The shear stress application is accomplished by removing or adding the pre-calculated weights on the two lower beams and by adjusting the hydraulic pressure in the load cell. All specimens are tested under the same magnitude of the mean stress (σ_m = 15 MPa), primarily to isolate the effect of confining pressure from the test results. The applied constant octahedral shear stresses range from 5.0, 8.0, 11.0 to 14.0 MPa. The major principal strain (ε_1), the intermediate principal strain (ε_2), the minor principal strain (ε_3) and the volumetric strain (ε_v) are calculated by:

$$\varepsilon_1 = \Delta L_1/L_1 \qquad (4.3)$$

$$\varepsilon_2 = \Delta L_2/L_2 \qquad (4.4)$$

$$\varepsilon_3 = \Delta L_3/L_3 \qquad (4.5)$$

$$\varepsilon_v = \varepsilon_1 + \varepsilon_2 + \varepsilon_3 \qquad\qquad (4.6)$$

where ΔL_1 is displacement of maximum principal stress direction, L_1 is width of specimen in maximum principal stress direction, ΔL_2 is displacement of intermediate principal stress direction, L_2 is width of specimen in intermediate principal stress direction, ΔL_3 is displacement of minimum principal stress direction and L_3 is width of specimen in minimum principal stress direction.

4.3.3 Test results

Figure 4.5 shows the strain-time curves for the three principal directions of salt specimens for mean normal stress (σ_m) 15 MPa of the octahedral shear stresses 5.0, 8.0, 11.0 and 14.0 MPa. The curves show the instantaneous, transient and steady-state creep phases.
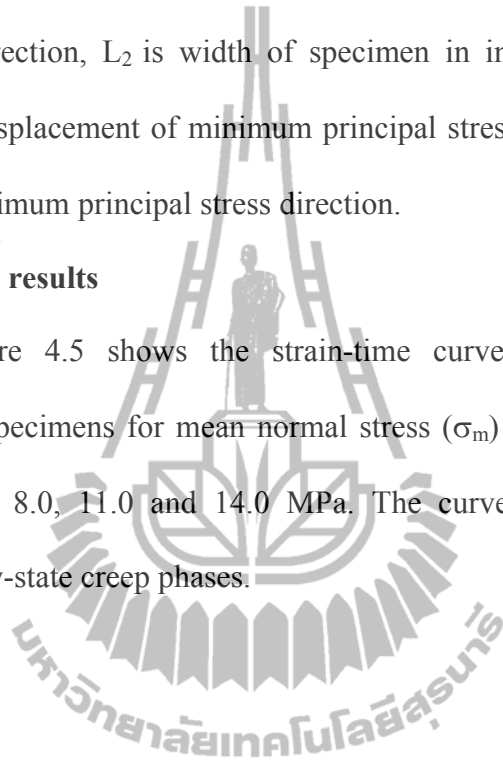
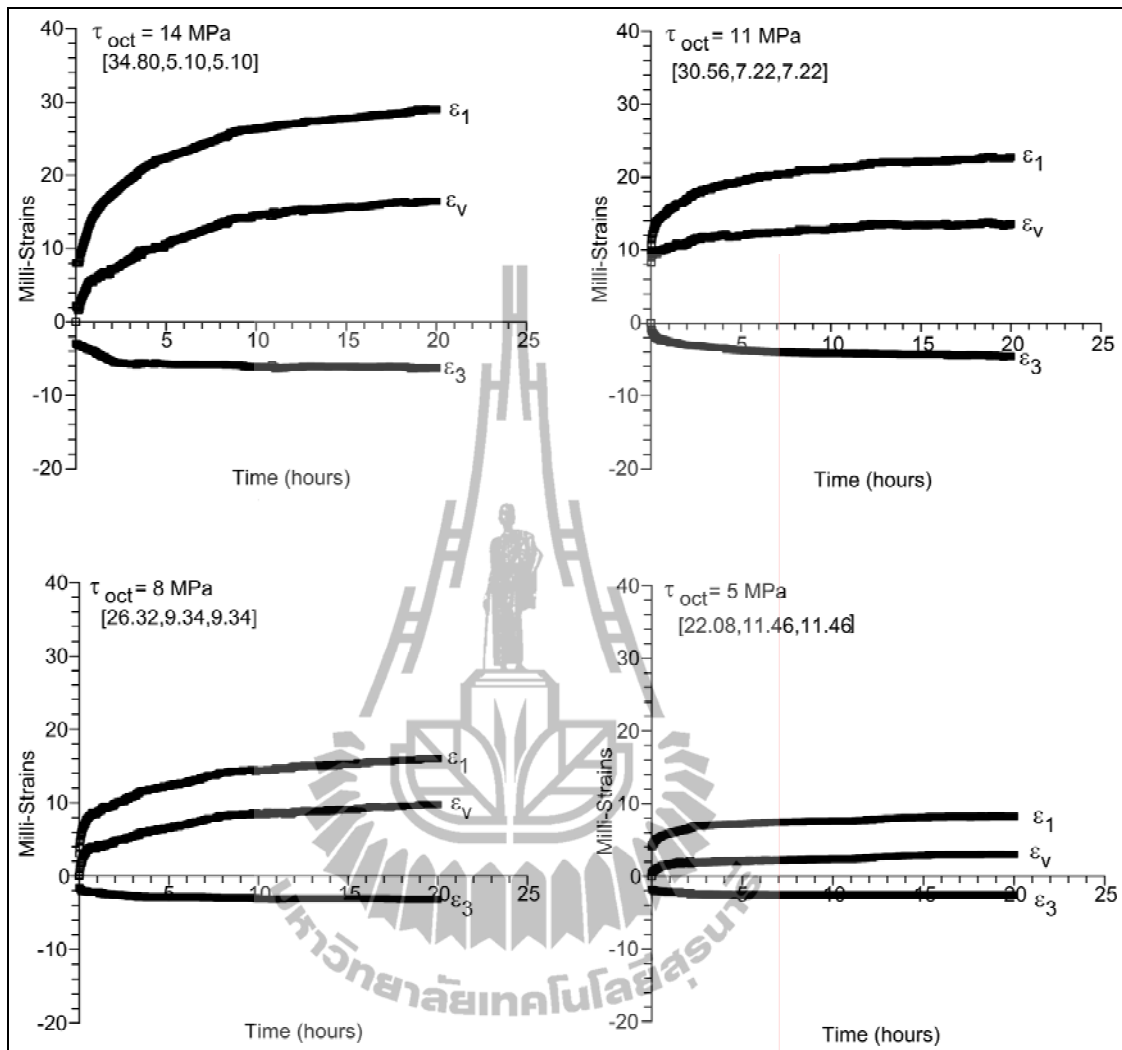**Figure 4.5** Strain-time curves for the triaxial cyclic loading test.

4.3.4 Discussions

The octahedral shear strains (γ_{oct}) for the triaxial test conditions are plotted as a function of time in Figure 4.6. They are calculated by:

$$\gamma_{oct} = [((\varepsilon_1 - \varepsilon_2)^2 + (\varepsilon_1 - \varepsilon_3)^2 + (\varepsilon_2 - \varepsilon_3)^2) / 3]^{1/2} \tag{4.7}$$

where γ_{oct} is octahedral shear strain, ε_1 is the major principal strain, ε_2 is the intermediate principal strain, and ε_3 is the minor principal strain. The octahedral shear strains increase with τ_{oct} magnitudes.
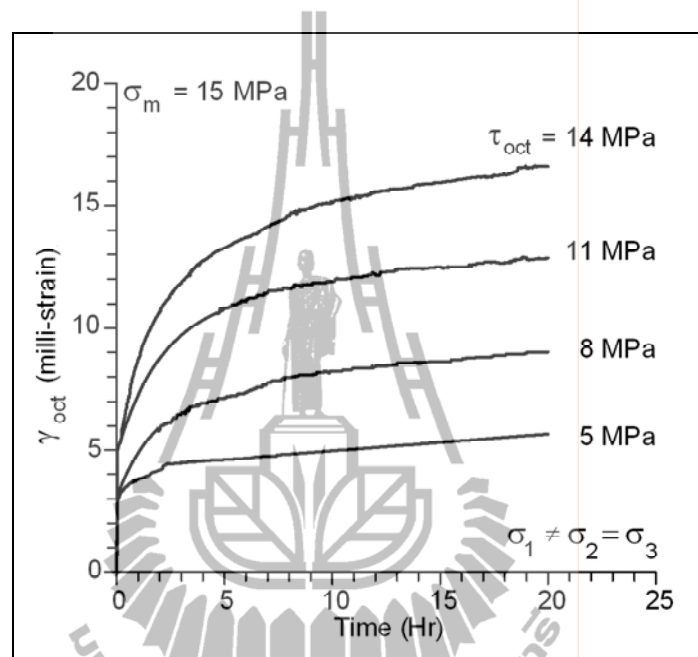
Figure 4.6 Octahedral shear strains plotted as a function of time for the triaxial cyclic loading of mean normal stress (σ_m) 15 MPa

4.4   True Triaxial Cyclic loading test

4.4.1   Test Procedure

The prepared rock specimen has nominal dimensions of 5.4×5.4×5.4 cm³. The test produce is similar to that of the previous except that

- Install hydraulic load cell on the middle of Between beam to apply cycles of load to cubical salt specimens.

- The lateral stresses were then decreased to the pre-defined minimum principal stress while the axial stress was increased pre-defined maximum principal

stress (by hydraulic load cell under the middle of lower beam) with in 30 seconds then axial stress (σ_1) was decreased to the mean stress (σ_m) and lateral stresses (σ_3) was increased to the mean stress (σ_m) with in 30 seconds and intermediate principal stress (σ_2) equivalent to the pre-defined mean stress (σ_m) to complete one cycle.

The applied stresses are then changed to obtain the pre-defined octahedral shear stresses (τ_{oct}) while maintaining the mean normal stress (σ_m) of 10, 15, 20 MPa (Table4.1)

**Table 4.1** Test parameters for the true triaxial cyclic loading test and the triaxial cyclic loading test.

Test conditions $\sigma_1 \neq \sigma_2 \neq \sigma_3$	σ_1 (MPa)	σ_2 (MPa)	σ_3 (MPa)	τ_{oct} (MPa)
$\sigma_m = 20$ MPa $\sigma_1 \neq \sigma_2 \neq \sigma_3$	37.2	20	2.8	14.0
	33.5		6.5	11.0
	29.8		10.2	8.0
	26.2		13.8	5.0
$\sigma_m = 15$ MPa $\sigma_1 \neq \sigma_2 \neq \sigma_3$	28.5	15	1.5	11.0
	24.8		5.2	8.0
	21.2		8.8	5.0
	17.5		12.5	2.0
$\sigma_m = 10$ MPa $\sigma_1 \neq \sigma_2 \neq \sigma_3$	18.6	10	1.4	7.0
	16.1		3.88	5.0
	12.4		7.55	2.0
$\sigma_m = 15$ MPa $\sigma_1 \neq \sigma_2 = \sigma_3$	34.8	5.1	5.1	14.0
	30.5	7.2	7.2	11.0
	26.3	9.3	9.3	8.0
	22.1	11.4	11.4	5.0

4.4.2 Test results

Figures 4.7, 4.8, and 4.9 show the strain-time curves for the three principal directions of salt specimens for mean normal stress (σ_m) 10, 15, 20 MPa. The curves show the instantaneous, transient and steady-state creep phases. These strains increase with τ_{oct} magnitudes and mean normal stress (σ_m).

4.4.3 Discussions

These strains increase with τ_{oct} magnitudes and mean normal stress (σ_m). The octahedral shear strains (γ_{oct}) for the true triaxial test conditions are plotted as a function of time in Figure 4.10, 4.11, and 4.12
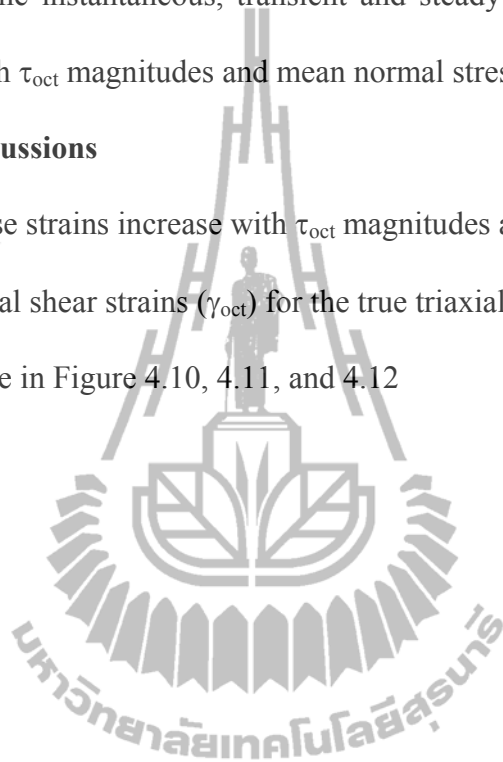
Figure 4.7 Strain-time curves for the true triaxial cyclic loading test of mean normal

stress (σ_m) 10 MPa. Numbers in blanket indicate
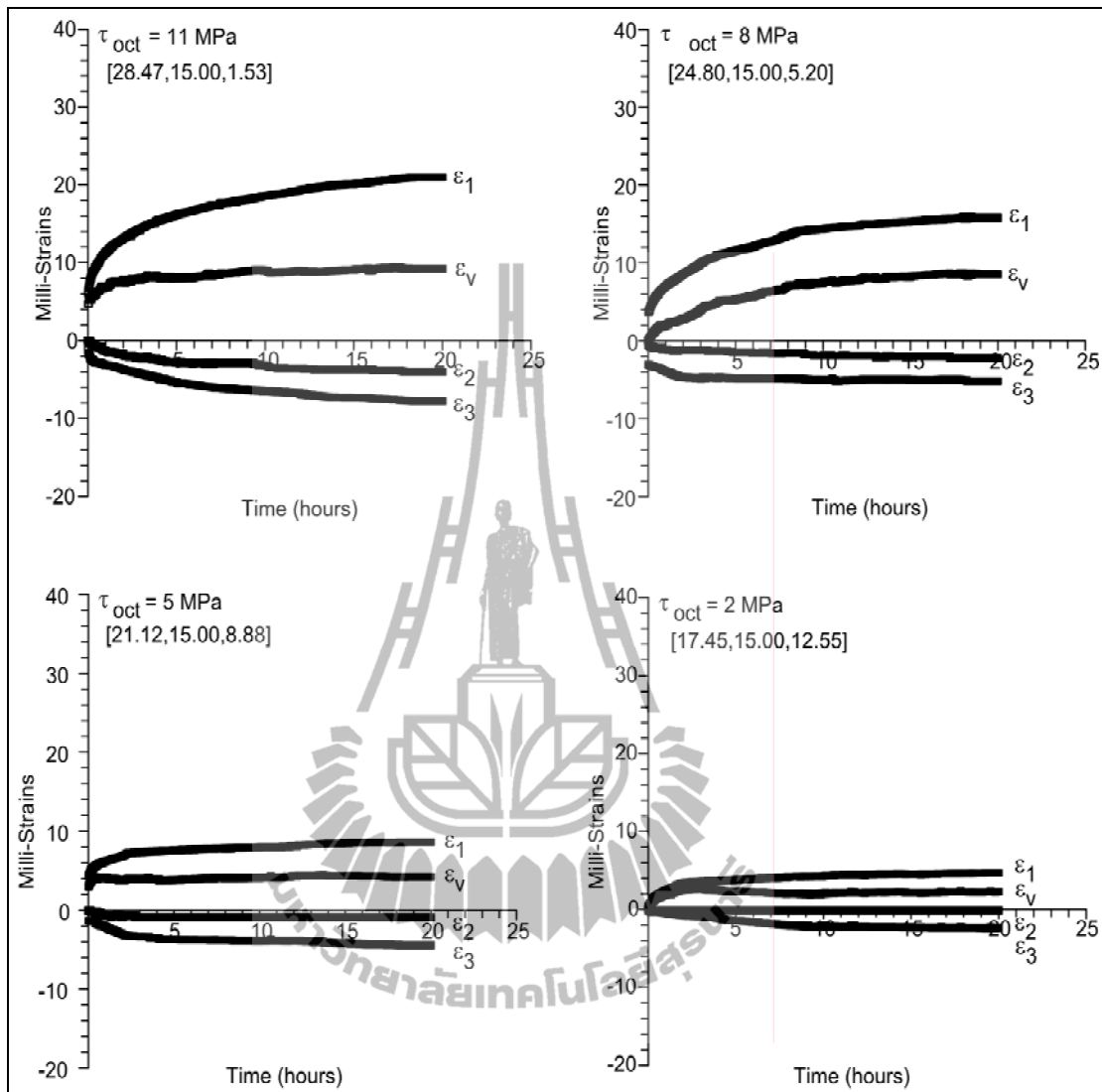
Figure 4.8 Strain-time curves for the true triaxial cyclic loading test of mean normal

stress (σ_m) 15 MPa. Numbers in blanket indicate
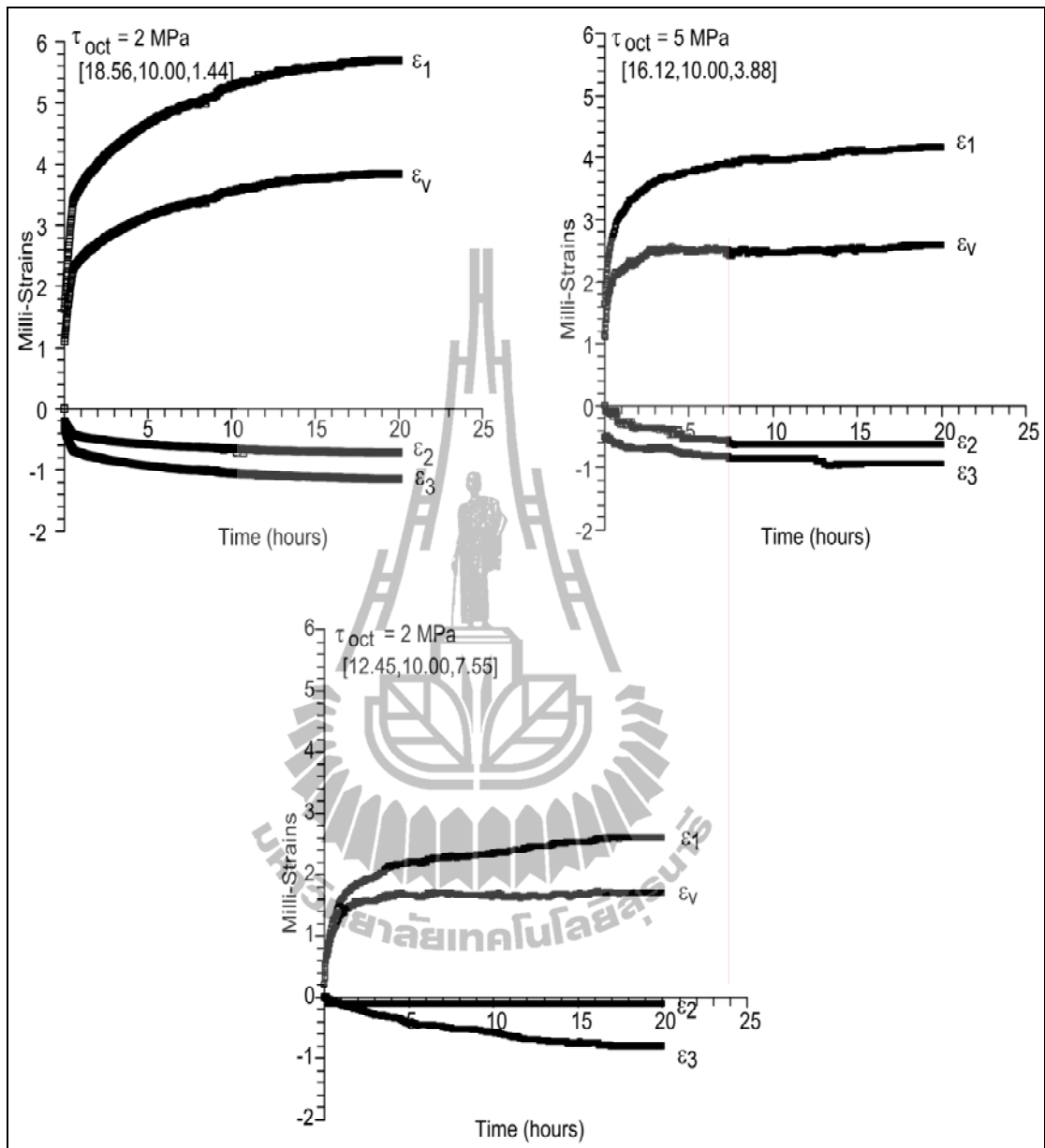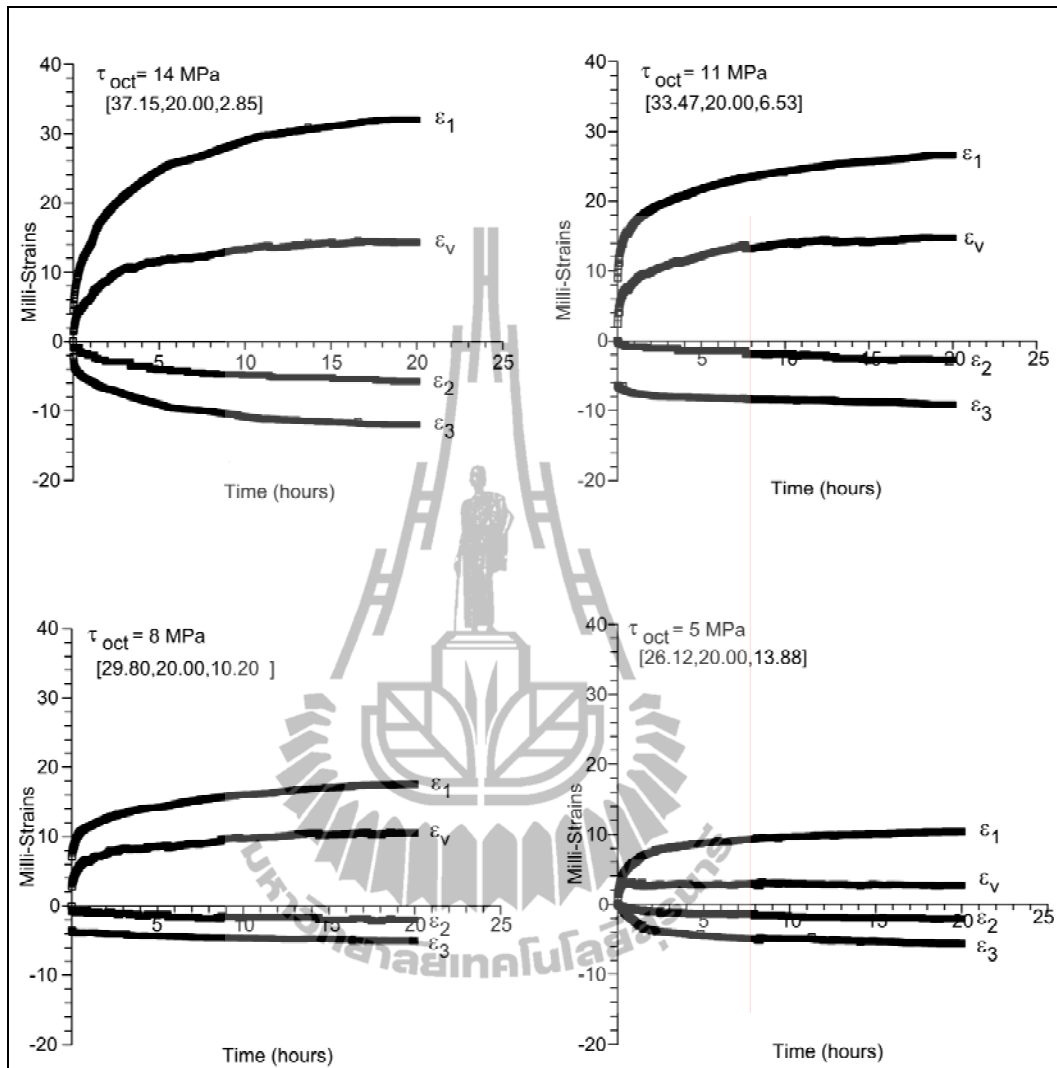
Figure 4.9 Strain-time curves for the true triaxial tyclic loading test of mean normal

stress (σ_m) 15 MPa. Numbers in blanket indicate
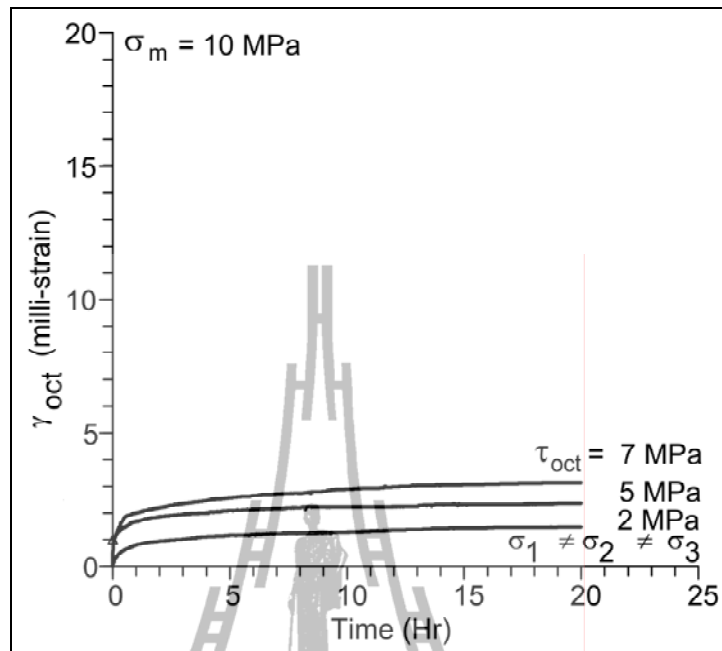
Figure 4.10 Octahedral shear strains plotted as a function of time for the true

triaxial cyclic loading of mean normal stress (σ_m) 10 MPa.
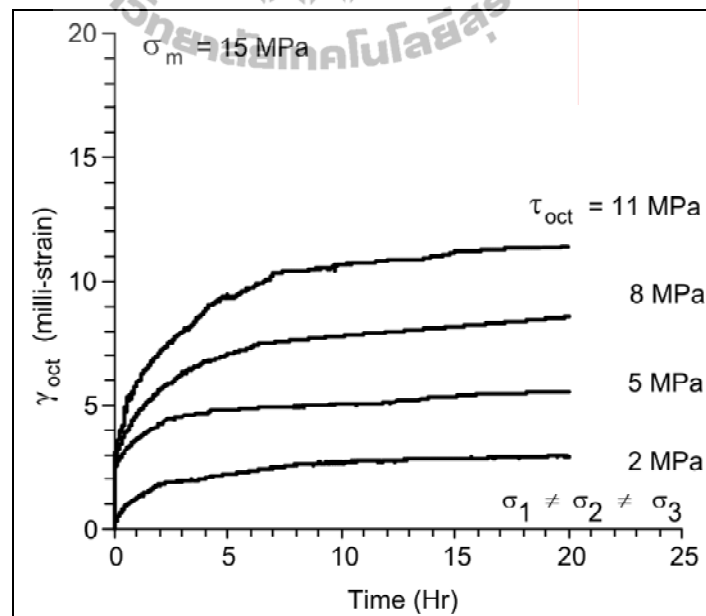
Figure 4.11 Octahedral shear strains plotted as a function of time for the true triaxial

cyclic loading of mean normal stress (σ_m) 15 MPa.

Figure 4.12 Octahedral shear strains plotted as a function of time for the true

triaxial cyclic loading of mean normal stress (σ_m) 20 MPa.

CHAPTER V

SALT PROPERTIES CALIBRATION

5.1 Introduction

The purpose of this chapter is to describe the calibration of salt property parameters. The regression analysis on the linear visco-elastic equation of the Burgers model is employed in the calibration. The data used in the calibration are obtained from t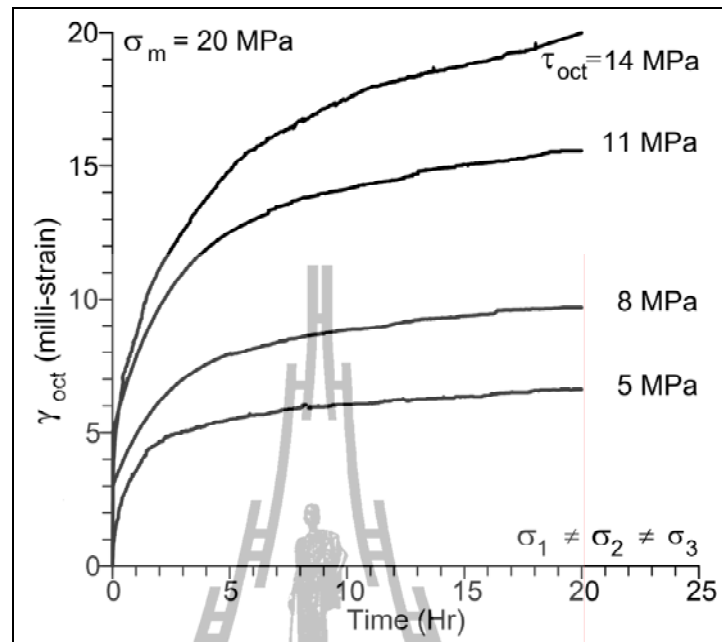he polyaxial creep tests and the polyaxial cyclic loading test. These parameters include the elastic modulus, the viscoelastic and the viscoplastic coefficients. The elastic and time-dependent parameters from the polyaxial cyclic loading results are compared with those calibrated from the conventional the polyaxial creep.

5.2 Calibration from tests

The objective of the calibration is to determine the properties parameters of the polyaxial creep tests and polyaxial cyclic loading. The time-related parameters are monitored, recorded and analyzed. Results from the polyaxial creep tests and polyaxial cyclic loading provide the data basis for the time-dependent properties on rock salt based on the conventional approach. A simple rheological creep model is used to describe behavior of the salt, i.e., Burgers Model. The regression analysis is with SPSS software used to calibration. The relation between the octahedral shear stress (τ_{oct}) and octahedral shear strain (γ_{oct}) are determined. The octahedral shear strains (γ_{oct}) for test conditions are plotted as a function of time. They are calculated by

$$\gamma_{oct} = [1/3][((\varepsilon_1 - \varepsilon_2)^2 + (\varepsilon_1 - \varepsilon_3)^2 + (\varepsilon_2 - \varepsilon_3)^2)]^{1/2} \qquad (5.1)$$

where γ_{oct} is the octahedral shear strain, ε_1 is the major principal strain, ε_2 is the intermediate principal strain, and ε_3 is the minor principal strain.

The linear elastic relation between octahedral shear strain and stress can be written as (Jaeger & Cook, 1979):

$$\gamma_{oct} = \tau_{oct} / 2G \qquad (5.2)$$

where τ_{oct} is the octahedral shear stress and G is the shear modulus.

Using the Laplace transformation a linear visco-elastic relation can be derived from the above equation as follows (Jaeger & Cook, 1979):

$$\gamma_{oct}(t) = \tau_{oct}(t)\left[\frac{1}{E_1} + \frac{t}{\eta_1} + \frac{1}{E_2}\exp\left(\frac{-E_2 t}{\eta_2}\right)\right] \qquad (5.3)$$

where $\gamma_{oct}(t)$ is octahedral shear strain which is a function of time, t is the elapse time, E_1 is the elastic modulus, E_2 and η_2 are the visco-elastic parameters and η_1 is visco-plastic parameter. Figure 5.1 shows the modular components of the Burgers model.
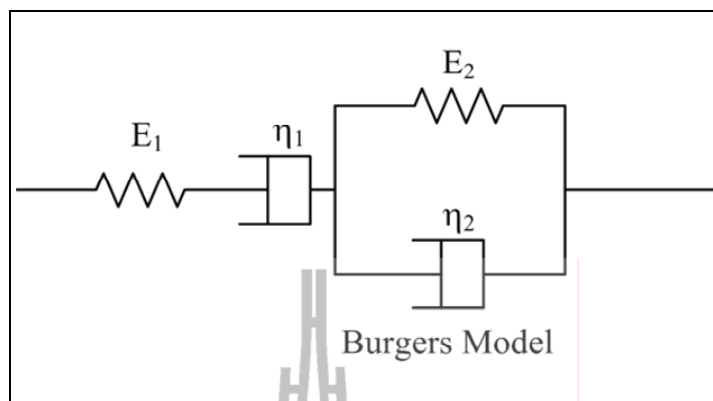
Figure 5.1 The modular components of the Burgers model.

Regression analyses are performed on the strain-time data using the SPSS statistical software (Wendai, 2000) to determine the Burgers parameters for each salt specimen. Table 5.1 shows the Burgers parameters calibrated from polyaxial cyclic loading tests. Table 5.2 shows the Burgers parameters calibrated from the polyaxial creep tests (Samsri et al., 2011)

Table 5.1 Burgers parameters calibrated from the polyaxial cyclic loading tests.

Test conditions $\sigma_1 \neq \sigma_2 \neq \sigma_3$	τ_{oct} (MPa)	E_1 (GPa)	E_2 (GPa)	η_1 (GPa.day)	η_2 (GPa.day)	μ
σ_m=20 MPa	14.0	20.0	1.35	1.69	0.05	0
	11.0	21.2	1.10	2.99	0.02	0
	8.0	22.1	1.30	2.69	0.05	0
	5.0	18.9	1.05	2.49	0.04	0
σ_m=15 MPa	11.0	20.3	1.60	2.19	0.06	0
	8.0	21.0	1.40	1.90	0.04	0
	5.0	22.0	1.25	1.80	0.03	0
	2.0	19.7	1.10	1.60	0.03	0
σ_m=10 MPa	7.0	19.0	4.00	3.50	0.04	0
	5.0	20.6	3.50	2.70	0.04	0
	2.0	20.0	2.50	2.00	0.06	0

Table 5.1 Burgers parameters calibrated from the polyaxial cyclic

loading tests (continued).

Test conditions $\sigma_1 \neq \sigma_2 = \sigma_3$	τ_{oct} (MPa)	E_1 (GPa)	E_2 (GPa)	η_1 (GPa.day)	η_2 (GPa.day)	μ
	14.0	20	1.45	4.15	0.04	1
	11.0	17	1.30	4.30	0.05	1
σ_m=15 MPa	8.0	18	1.50	3.78	0.04	1
	5.0	19	1.45	3.00	0.01	1

Table 5.2 Burgers parameters calibrated from the polyaxial creep tests

(Samsri et al., 2011)

Test conditions	τ_{oct} (MPa)	E_1 (GPa)	E_2 (GPa)	η_1 (GPa.day)	η_2 (GPa.day)	μ
	14	19.7	1.10	30.6	0.031	1
$\sigma_1 \neq \sigma_2 \neq \sigma_3$	11	19.4	1.00	33.1	0.029	1
	8	19.0	0.91	30.9	0.026	1
	5	19.2	0.99	29.2	0.022	1
	14	19.5	1.20	31.3	0.033	0.75
$\sigma_1 \neq \sigma_2 = \sigma_3$	11	19.1	1.30	31.8	0.028	0.84
	8	19.5	0.85	25.2	0.025	0.78
	5	20.1	0.80	26.7	0.021	0.18

Figure 5.2 shows the Burgers parameters as a function of the lode parameter.
The lode parameters are calculated by

$$\mu = -\left[\frac{2\sigma_2 - \sigma_3 - \sigma_1}{\sigma_1 - \sigma_3}\right] \tag{5.4}$$

where μ is the lode parameter, σ_1 is the major principal stress, σ_2 is the intermediate

principal stress, and σ_3 is the minor principal stress.
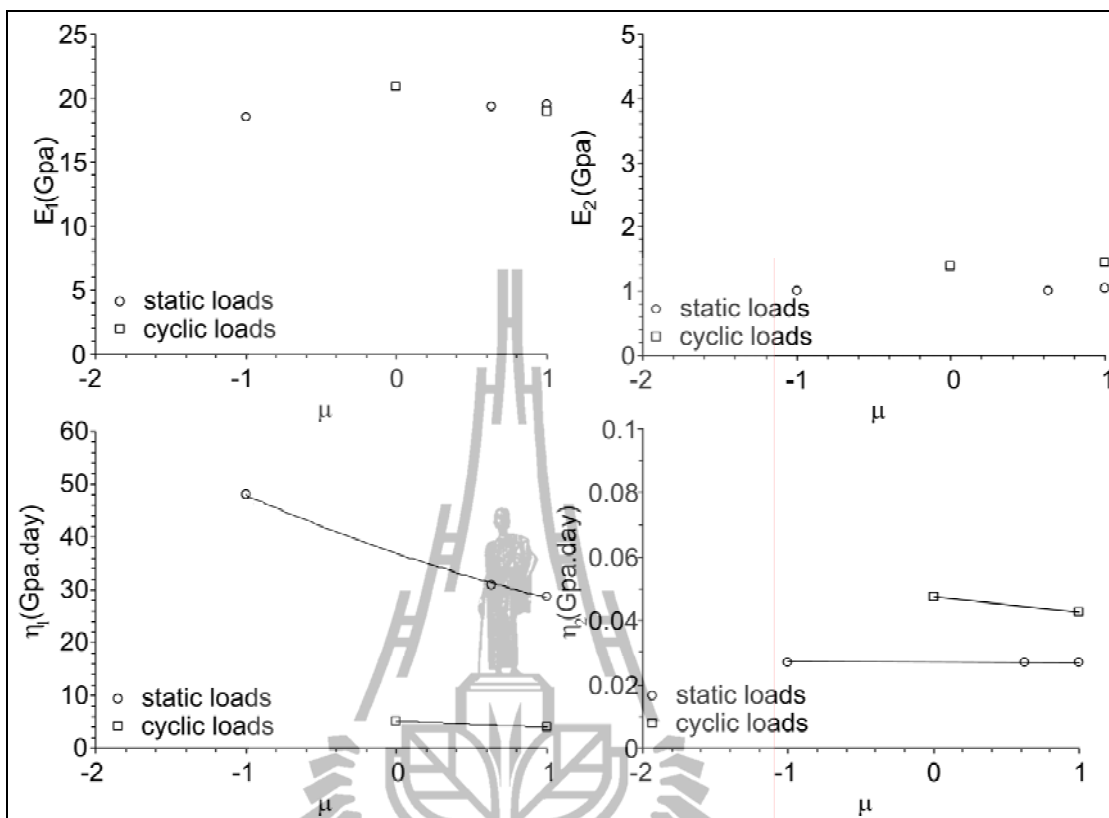
Figure 5.2 The Burgers parameters as a function of the lode parameter.

5.3 Discussions

The time-dependent parameters from the polyaxial cyclic loading tests results are compared with those calibrated from the conventional creep methods. The salt elastic parameters (E_1, E_2) and visco-elastic parameters (η_2) tends to be independent of the cyclic loads. In the steady-state creep phase, the visco-plastic parameter (η_1) calibrated from the the polyaxial cyclic loads test is about an order of magnitude lower than those under true triaxial static loads. This suggests that the cyclic loading condition can accelerate the visco-plastic creep of the salt.

CHAPTER VI

COMPUTER SIMULATIONS

6.1 Introduction

This chapter describes the finite difference analyses using FLAC (Itasca, 1992) to demonstrate the impact of cyclic loading on the salt behavior around a gas storage cavern. The time-dependent parameters from the polyaxial cyclic loading tests and the conventional creep methods are used in the computer simulation.

6.2 Numerical simulations

A finite difference analysis with the creep model above was performed to demonstrate the impact of cyclic loading on the salt behavior around a natural gas storage cavern in rock salt subject to daily cycles of pressure injection and retrieval. For this demonstration, the cavern is taken as an upright cylinder with a diameter of 50 m. The top and bottom of the cavern are assumed at 500 m and 1000 m depths. The analysis is made in axis symmetry under isothermal condition and assuming that no nearby underground structure within 500 m radius. The cavern model is shown in Figure 6.1. The storage cavern model is subject to the internal pressures of 20% (3 MPa) and of the in-situ stress at the cavern. The internal pressures are assumed to be uniform on the cavern boundaries. The elastic modulus and Poisson's ratio for the salt are taken as 21.5 GPa and 0.4, respectively (Sriapai and Fuenkajorn, 2010). Four sets of property parameters are used in the simulation, which are calibrated from the triaxial cyclic loading tests, the true triaxial cyclic loading tests, the triaxial creep tests

and the true triaxial creep tests under the mean stresses (σ_m) of 15 MPa. This is because the cavern depth is between 500 m and 1000 m, which is equivalent to the mean stresses (σ_m) of 15 MPa. Table 6.1 gives a summary of the parameters used in numerical simulation.

Table 6.1 Material properties used in FLAC simulations.

Parameters	1*	2*	3*	4*
Elastic modulus, E (GPa)	21.5	21.5	21.5	21.5
Possion' ratio, ν	0.4	0.4	0.4	0.4
Friction angle, ϕ (Degrees)	50.0	50.0	50.0	50.0
Cohesion, c (MPa)	5.0	5.0	5.0	5.0
Density, ρ (g/cc)	2.2	2.2	2.2	2.2
Internal pressures (MPa)	3.0	3.0	3.0	3.0
Spring constant in visco-elastic phase, E_2 (GPa)	1.43	1.38	1.03	1.00
Visco-plastic coefficient in steady-state phase, η_1 (GPa.Day)	3.94	5.21	28.75	30.95
Visco-elastic coefficient in transient phase, η_2 (GPa.Day).	0.042	0.047	0.026	0.027

Remark : 1* = triaxial cyclic loading tests   2* = true triaxial cyclic loading tests

3* = triaxial creep tests   4* = true triaxial creep tests

6.3 Results

The FLAC simulations determine that the cavern closure simulated using parameters calibrated from the cyclic loading test results is greater than those from the static loading results. The parameters calibrated from the triaxial condition test results are greater than those from the true triaxial (polyaxial) condition, as shows in Figure 6.2 shows the diameter closure at depth of 1000 m as function of time. This suggests that determination of the cavern closure using the parameters calibrated from the conventional creep testing may not conservative.
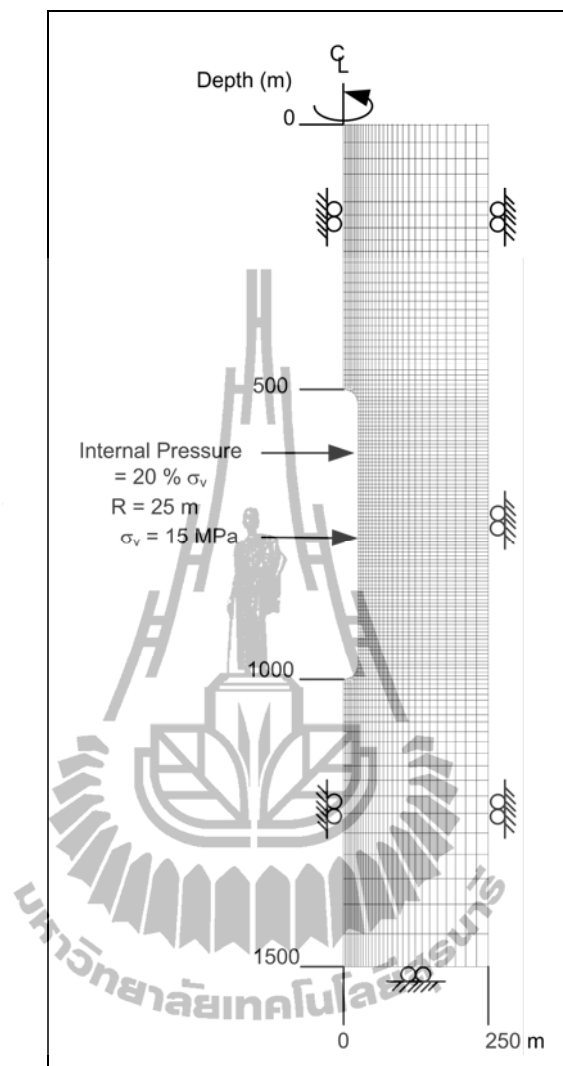
Figure 6.1 Finite difference mesh constructed to simulate a gas storage cavern
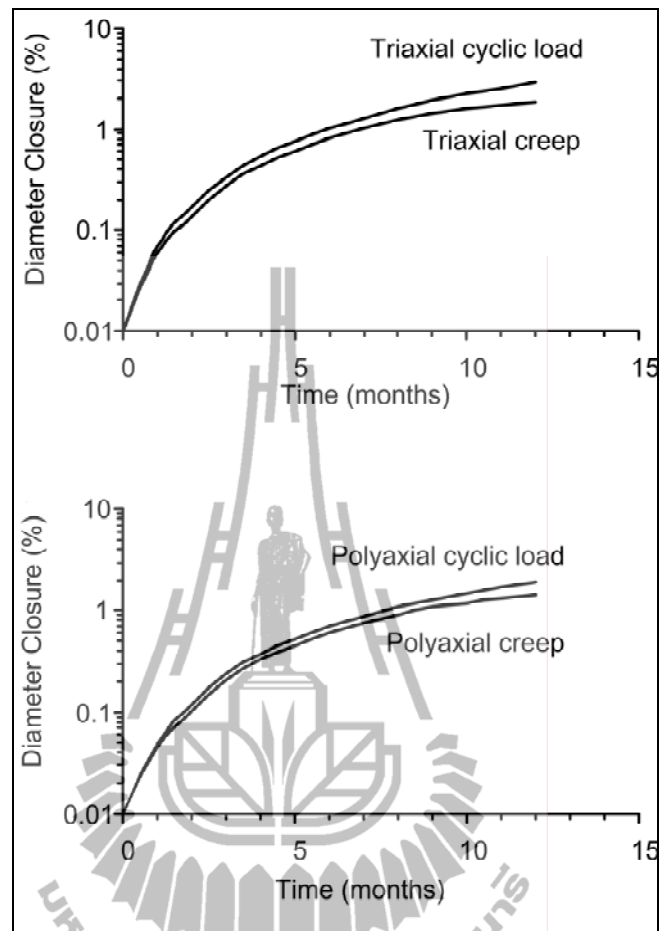
in the Maha Sarakham salt.

Figure 6.2 Cavern closure using parameters from static and cyclic loading tests.

CHAPTER VII

DISCUSSIONS, CONCLUSIONS AND

RECOMMENDATIONS FOR FUTURE STUDIES

7.1   Discussions and conclusions

The objective of this research is to determine the effect of cyclic loading on the time-dependent behavior of rock salt under true triaxial stresses. A polyaxial load frame is used to apply cycles of principal stresses to the cubical salt speciems. The applied stresses are varied from the triaxial ($\sigma_1 \neq \sigma_2 = \sigma_3$) condition to the polyaxial ($\sigma_1 \neq \sigma_2 \neq \sigma_3$) conditions. The results are used to calibrate the elastic, visco-elastic and visco-plastic parameters of the rock and compared with those determined from the conventional static loading creep tests.

The Burgers model is used to describe the elastic, visco-elastic (transient) and visco-plastic (steady-state) behavior of the salt. Regression analyses on the octahedral shear strain - time curves suggest the elastic deformation of salt, described by E_1 is not affected by the cyclic loads. In the steady-state creep phase, the visco-plastic coefficients calculated from the cyclic loading test are about an order of magnitude lower than those under static loading. The spring constant in visco-elastic phase, (E_2) and visco-elastic parameters (η_2) tends to be independent of the cyclic loads which agree with the experimental results obtained by Fuenkajorn and Phueakphum (2010). The visco-plastic parameter, η_1 depend on the intermediate principal stress, σ_2 which

agree with the test results obtained by Samsri et al. (2010). It when the intermediate principal stress increases.

The cavern closure simulated using parameters calibrated from the cyclic loading test results are greater than those from the static loading results and parameters calibrated from triaxial condition test results are greater than those from the true triaxial condition This suggests that application of the property parameters obtained from the conventional static loading creep test to assess the stability of the storage caverns with internal pressure fluctuation may not be conservative.

The intermediate principal stress affects the visco-plastic coefficients by strengthening the salt matrix. The cyclic loads casese an accumulation of the plastic (time-dependent) strains during each cycle of loading and hence accelerate the total creep strain. This why parameter, η_1 is lower under cyclic loading compared to under static loading.

7.2 Recommendations for future studies

The test specimens here are relatively small. Testing on larger specimens is desirable to confirm the research findings. Testing time should be increased to obtain a longer trend of the strain-time curves in the visco-plastic phase, hence revealing clearer effects of the cyclic loads and the intermediate principal stress. The uncertainties and adequacies of the research investigation and results discussed above lead to the recommendations for further studies. The effect of friction at the interface between the loading platen and rock surfaces should also be investigated. The effect of temperature and frequency should be considered on the true triaxial cyclic loading tested as they play a significant role on salt around storage caverns. The constitutive

law used in this study is a linear visco-elastic model and may not be adequately describe the salt behavior. Other non-linear constitutive laws, such as power laws and structural laws may be needed to describe the salt behavior.

REFERENCES

ASTM D2664-95a. Standard test method for triaxial compressive strength of undrained rock core specimens without pore pressure measurements. In **Annual Book of ASTM Standards** (Vol. 04.08). Philadelphia: American Society for Testing and Materials.

ASTM D2938-95. Standard test method for unconfined compressive strength of intact rock core specimens. In **Annual Book of ASTM Standards** (Vol. 04.08). Philadelphia: American Society for Testing and Materials.

ASTM D3967-95a. Standard test method for splitting tensile strength of intact rock core specimens. In **Annual Book of ASTM Standards** (Vol. 04.08). Philadelphia: American Society for Testing and Materials.

Aubertin, M., Gill, D. E. and Ladanyi, B. (1992). Modeling the transient inelastic flow of rock salt. In **Proceedings of the Seventh Symposuim on Salt** (vol. 1, pp. 93-104). Elsevier Science Pub.

Aubertin, M., Julien M. R., Servant, S. and Gill, D. E. (1999). A rate-dependent model for the ductile behavior of salt rocks. **Canadian Geotechnical Journal.** 36(4): 660-674.

Aubertin, M., Sgaoula, J. and Gill, D. E. (1992). A damage model for rock salt: Application to tertiary creep. In **Proceedings of the Seventh Symposuim on Salt** (vol. 1, pp. 117-125). Elsevier Science Pub.

Aubertin, M., Sgaoula, J. and Gill, D. E. (1993). Constitutive modeling of rock salt: Basic considerations for semi-brittle behavior. In **Proceedings of the Fourth International Symposuim on Plasticity and It's Current Applications** (pp. 92). Baltimore.

Aubertin, M., Sgaoulla, J., Servant, S., Julien, M. R., Gill, D. E. and Ladanyi, B. (1998). An upto-date version of SUVIC-D for modeling the behavior of salt. In **Proceedings of the Fourth Conference on the Mechanical Behavior of Salt** (pp. 205-220). Clausthal,Germany: Trans Tech Publications.

Chokski, A. H. and Langdon, T. G. (1991). Characteristics of creep deformation in ceramics. **Materails Science and Technology** 7: 577-584.

Cristescu, N. D. (1991). Non-associated elastic/visco-plastic constitutive equations for sand. **Int. J. Plasticity** 7: 41-64.

Cristescu, N. D. (1993a). Constitutive equation for rock salt and mining applications. In **Proceedings of the Seventh symposium on salt** (Vol. 1, pp. 105-115). Amsterdam: Elsevier Science Publishers B. V.

Cristescu, N. D. (1993b). A general constitutive equation for transient and stationary creep of rock salt **Int. J. Rock Mech. Sci. & Geomech. Abstr.** 30 (2): 125-140

Cristescu, N. D. (1994a). A procedure to determine nonassociated constitutive equations for geomaterials. **Int. J. Plasticity** 10: 103-131.

Cristescu, N. D. (1994b). **Viscoplasticity of geomaterials.** Visco-Plastic Behaviour of Geomaterials. Springer Verlag, Vienna, pp. 103-207.

Cristescu, N. D. (1996). Stability of large underground caverns in rock salt. In **Proceedings of the 2nd Symposium, North American Rock Mechanics** (pp. 101-108). Canada: A. A. Balkema.

Dusseault, M.B. and Fordham, C.J. (1993). Time-dependent behavior of rocks. **Comprehensive Rock Engineering Principles, Practice and Project: Rock Testing and Site Characterization** (Vol. 3, pp. 119-149). London, Pergamon.

Fokker, P. A. (1995). **The behavior of salt and salt caverns**. Ph.D Thesis, Delft University of Technolgoy.

Fokker, P. A. (1998). The micro-mechanics of creep in rock salt. In **Proceedings of the Fourth Conference on the Mechanical Behavior of Salt** (pp. 49-61). Clausthal-Zellerfeld, Germany: Trans Tech Publications.

Fokker, P. A. and Kenter, C. J. (1994). The micro mechanical description of rock salt plasticity. In **Eurock'94** (pp. 705-713). Rotterdam: Balkema.

Fokker, p. A. and Kenter, c. J. (1994). The micro mechanical description of rock salt plasticity. In **Eurock'94** (pp. 705-713). Rotterdam: Balkema.

Franssen, R. C. M. and Spiers, C. J. (1990). Deformation of polycrystalline salt in compression and in shear at 250-350 C. **Deformation Mechanisms, Rheology and Tectonics, Geological Society Special Publication** 45: 201-213.

Fuenkajorn, K. and Daemen, J. J. K. (1988). **Boreholes closure in salt**. Technical Report Prepared for The U.S. Nuclear Regulatory Commission. Report No. NUREG/CR-5243 RW. University of Arizona.

Fuenkajorn, K. and Phueakphum, D. (2010). Effects of cyclic loading on mechanical properties of Maha Sarakham salt. **Engineering Geology** 112: 43-52.

Fuenkajorn, K. and Serata, S. (1992). Geohydrological integrity of CAES in rock salt. In **Proceedings of the Second International Conference on Compressed-Air Energy Storage** (pp. 4.1-4.21). San Francisco, CA: Electric Power Research Institute.

Fuenkajorn, K. and Serata, S. (1994). Dilation-induced permeability increase around caverns in rock salt. In **Proceeding of the 1st North American Rock Mechanics Symposium** (pp. 648-656). Rotterdam: A. A. Balkema.

Jaeger, J.C., and Cook, N.G.W. (1979). **Fundamentals of Rock Mechanics (3rd. Edn.)**. Chapman & Hall, London, pp. 105-106.

Jeremic, M. L. (1994). **Rock mechanics in salt mining** (530 pp.). Rotherdam: A. A. Balkema.

Jin, J. and Cristescu, N. D. (1998). An elastic/visco-plastic model for transient creep of rock salt. **International Journal of Plasticity** 14 (1-3): 85.

Jin, J., Cristescu, N. D. and Hunche, บ. (1998). A new elastic/visco-plastic model for rock salt, In **Proceedings of the Fourth Conference on the Mechanical Behavior of Salt** (pp. 249-262). Clausthal-Zellerfeld, Germany: Trans Tech Publications.

Knowles, M. K., Borns, D., Fredrich, J., Holcomb, D., Price, R. and Zeuch, D. (1998). Testing the disturbed zone aroud a rigid inclusion in salt. In **Proceedings of the Fourth Conference on the Mechanical Behavior of Salt** (pp. 175-188). Clausthal, Germany: Trans Tech Publications.

Korthaus, E. (1996). Measurement of crushed salt consolidation under hydrostatic and deviatoric stress conditions. **In Proceedings of the Third Conference on the Mechanical Behavior of Salt** (pp. 311-322). Clausthal-Zellerfeld, Germany: Trans Tech Publications.

Korthaus, E. (1998). Consolidation and deviatoric deformation behavior of dry crushed salt at temperatures up to 150 °c. **In Proceedings of the Fourth Conference on the Mechanical Behavior of Salt** (pp. 365-378). Clausthal-Zellerfeld, Germany: Trans Tech Publications.

Massier, D. (1996). Rate type constitutive equations with applications to the calculus of the stress state and of the displacement field around cavities in rock salt. In **Proceedings of the Third Conference on the Mechanical Behavior of Salt** (pp. 545-558). Clausthal-Zellerfeld, Germany: Trans Tech Publications.

Munson, D. E. and Wawersik, W. R. (1993). Constitutive modeling of salt behavior – State ofthe technology. In **Proceedings of the Seventh International Congess on Rock Mechanics** (vol. 3, pp. 1797-1810). Balkema.

Pudewills, A. and Hornberger, K. (1996). A unified visco-plastic model for rock salt. In **Proceedings of the Third Conference on the Mechanical Behavior of Salt** (pp. 45-52). Clausthal-Zellerfeld, Germany: Trans Tech Publications.

Raj, S. V. and Pharr, G. M. (1992). Effect of temperature on the formation of creep substructure in sodium chloride single crystal. **American Ceramic Society** 75 (2): 347-352.

Samsri, P., Sriapai, T., Walsri ,C. and Fuenkajorn, K. (2010). Polyaxial creep testing of rock salt. In **Proceedings of the Third Thailand Symposium on Rock Mechanicson** (pp. 125-132). Thailand.

Senseny, P. E., Handin, J. W., Hansen, F. D. and Russell, J. E. (1992). Mechanical behavior of rock salt: phenomenology and micro-mechanisms. **International Journal of Rock Mechanics and Mining Sciences** 29 (4): 363-378.

Serata, S. and Fuenkajorn, K. (1992a). Formulation of a constitutive equation for salt. In **Proceedings of the Seventh International Symposium on Salt** (Vol. 1, pp. 483-488). Amsterdam: Eisevier Science.

Stormont, J. C. and Fuenkajorn, K. (1994). Dilation-induced permeability changes in rock salt. In **Proceedings of the 8th International Conf, Computer Methods and Advances in Geomechanics** (pp. 1296-1273). Morgantown, West Virginia.

Walsri, C., Poonprakon, P., Thosuwan R. and Fuenkajorn, K. (2009). Compressive and tensile strengths of sandstones under true triaxial stresses. In **Proceeding 2nd Thailand Symposium on Rock Mechanics**. Chonburi, Thailand. 2: 199-218.

Wanten, P. H., Spiers, C. J. and Peach, C. J. (1996). Deformation of NaCl single crystals at 0.27Tm < T < 0.44Tm. In **Proceedings of the Third Conference on the Mechanical Behavior of Salt** (pp. 117-128). Clausthal, Germany: Trans Tech Publications.

Warren, J. (1999). **Evaporites: Their Evolution and Economics** (pp.235-239). Blackwell Science. Oxford.

Wendai, L., 2000, **Regression analysis, liner regression and probit regression In 13 chapters**. SPSS for Windows: statistical analysis. Publishing House of Electronics Industry. Beijing.

BIOGRAPHY

Mr. Komkrit Phatthaisong was born on January 15, 1988 in Nakhon Ratchasima province, Thailand. He received his Bachelor's Degree in Engineering (Geotechnology) from Suranaree University of Technology in 2009. For his post-graduate, he continued to study with a Master's degree in the Geological Engineering Program, Institute of Engineering, Suranaree university of Technology. During graduation, 2009-2011, he was a part time worker in position of research assistant at the Geomechanics Research Unit, Institute of Engineering, Suranaree University of Technology.